Elliptic polarisation of the polar motion excitation

Christian Bizouard

Elliptic polarisation of the polar motion excitation

Christian Bizouard[1]

Abstract Because of its geophysical interpretation, Earth's polar motion excitation is generally decomposed into prograde (counter-clockwise) and retrograde (clockwise) circular terms at fixed frequency. Yet, these later are commonly considered as specific to the frequency and to the underlying geophysical process, and no study has raised the possibility that they could share features independent from frequency. Complex Fourier Transform permits to determine retrograde and prograde circular terms of the observed excitation and of its atmospheric, oceanic and hydrological counterparts. The total prograde and retrograde parts of these excitations are reconstructed in time domain. Then, complex linear correlation between retrograde and conjugate prograde parts is observed for both the geodetic excitation and the matter term of the hydro-atmospheric excitation. In frequency domain, the ratio of the retrograde circular terms with their corresponding conjugate prograde terms favours specific values: the amplitude ratio follows a probabilistic gamma distribution centred around 1.5 (maximum for 1), and the argument ratio obeys a distribution close to a normal law centred around $2\alpha = 160°$. These frequency and time domain characteristics mean an elliptical polarisation towards $\alpha = \sim 80°$ East with an ellipticity of 0.8, mostly resulting from the matter term of the hydro-atmospheric excitation. Whatsoever the frequency band above 0.4 cpd, the hydro-atmospheric matter term tends to be maximal in the geographic areas surrounding the great meridian circle of longitude $\sim 80°$ or $\sim 260°$ East. The favoured retrograde/prograde amplitude ratio around 1.5 or equivalently the ellipticity of 0.8 can result from the amplification of pressure waves propagating towards the west by the normal atmospheric mode Ψ_3^1 around 10 days.

Keywords Earth's rotation · Polar motion · Hydro-atmospheric excitation · Elliptical polarisation

✉ Christian Bizouard
christian.bizouard@obspm.fr

[1] Observatoire de Paris, SYRTE/UMR 8630, 77, avenue Denfert-Rochereau, 75014 Paris, France

1 Introduction

The wobble of the rotation pole at Earth's surface has been discovered more than 120 years ago. It is mostly composed of two counter-clockwise wobbles at periods of 433 days and 365 days with mean amplitude of 200 and 100 milli-arcseconds (mas), respectively. The other spectral components are at least 10 times smaller, as far as we overlook the secular polar displacement (400 mas per century). The predominance of these prograde components reflects the resonance at the 433-day period of the free mode, which is a counter-clockwise circular motion.

More precisely, let $p = x - iy$ be the complex pole coordinates referred to the terrestrial reference frame equatorial plane, χ the excitation function, angular momentum balance law expressed in the terrestrial reference frame yields after linearisation (see e.g. Munk and Mac Donald 1960; Brzeziński 1994; Bizouard 2014):

$$p + \frac{i}{\tilde{\sigma}_c}\dot{p} = \chi \tag{1}$$

where $\tilde{\sigma}_c = 2\pi/433(1-i/2Q)$ rad/day is the complex Chandler angular frequency, of which the small imaginary part accounts for Chandler wobble damping with a quality factor Q in the interval [40–200] that is a relaxation time between 20 and 80 years. The left-hand side is called equatorial geodetic excitation, because it can be derived directly from the geodetic determination of the pole coordinates. The right-

hand side χ, as far as the fluid layers are incorporated in the mechanical system, is proportional to the equatorial angular momentum increment caused by mass redistribution and motion relative to the terrestrial axes, mostly originating in the hydro-atmospheric layer. Therefore, they are called equatorial angular momentum function (AMF) or more simply geophysical excitation. They are composed of two terms: the matter term $\chi_{\rm ma}$ reflecting the mass redistribution at a given time, and the motion term $\chi_{\rm mo}$ caused by the mass motion with respect to Earth's surface.

$$\chi = \chi_{\rm ma} + \chi_{\rm mo}. \tag{2}$$

The matter term is directly proportional to the off-diagonal change $I_{13} + iI_{23}$ of the Earth inertia matrix expressed in the Terrestrial reference frame (TRF), and the motion term is proportional to the equatorial components h_1 and h_2 of the relative angular momentum:

$$\chi_{\rm ma} = \alpha_{\rm ma}\frac{I_{13} + iI_{23}}{C - A}, \quad \chi_{\rm mo} = \alpha_{\rm mo}\frac{h_1 + ih_2}{C - A}, \tag{3}$$

where $\alpha_{\rm ma} \sim 1.01$ and $\alpha_{\rm mo} \sim 1.6$ are coefficients rendering the effect of the Earth non-rigidity (Barnes et al. 1983). Because of these coefficients $\chi_{\rm ma}$ and $\chi_{\rm mo}$ are often termed as effective Angular Momentum function (AMF) or EAMF in contrast to simple AMF where these multiplicative factors are absent.

The common approach for studying the polar motion is to compare the geodetic excitation χ_G with the geophysical excitation χ mostly reconstructed from models of the global circulation taking place in the hydro-atmosphere. At sub-secular time scales, other influences are possible, like core-mantle electromagnetic coupling and Earthquake mass redistribution, but have never been clearly evidenced.

Now, considering (1) in frequency domain, that is

$$p(\sigma) = -\frac{\tilde{\sigma}_c}{\sigma - \tilde{\sigma}_c}\chi(\sigma) = T(\sigma)\chi(\sigma), \tag{4}$$

the interest of splitting prograde and retrograde components is evident, for prograde terms having periods close to 433 days are amplified, while transfer function $T(\sigma)$ of the retrograde terms has a module smaller than 1, tending towards 0 with increasing absolute value of the frequency. Within this frequency domain approach, prograde and retrograde terms of the excitation are considered as specific to the frequency, and are estimated in light of their effect on polar motion. To our knowledge, no study has ever raised the question to know whether the prograde and retrograde terms could be interrelated independently from the frequency. Could it be that, whatever be the frequency, the elliptical path resulting from the addition of prograde and retrograde terms, presents the same privileged direction?

It had been noted in studies going back to the early twentieth century (Sidorenkov 2009; Munk and Mac Donald 1960; Lambeck 1980) that the annual geodetic excitation is an ellipse, which the semi-major axis has a stable ellipticity and longitude (80°–90° East). The same characteristics was found later in the atmospheric excitation (Lambeck 1980). We can extend the computation of ellipticity (or retrograde to prograde term ratio) and longitude of the semi-major axis to the whole set of frequencies representing the polar motion and its excitation. And, as surprising it will be for a specialist of Earth's rotation, we aim at showing that the obtained values tend to privilege the 80°–90° East polarisation, and a mean ellipticity of about 0.8.

2 Data

We treat consistent angular momentum function time series resulting from coupled global circulation model of the hydro-atmosphere.

First, we consider the atmospheric EAMF of the NCEP/NCAR (National Center for Environmental Prediction/National Center of Atmospheric Research) over the period 1949–2014, as provided by the Global Geophysical Fluids Center of the IERS (SBA 2015); they are coupled with oceanic EAMF of the ECCO-MIT (SBO 2015) (1949–2014) and hydrological EAMF of the CPC model (1948–2007) (SBH 2015). In the following, we shall report to these series as NCEP, ECCO and CPC, respectively.

The second hydro-atmospheric series are the European Centre for Medium Range Weather Forecasts (ECMWF) atmospheric EAMF, the oceanic EAMF estimated from the Ocean Model for Circulation and Tides (OMCT) and the land fresh water of the Land Surface Discharge Model (LSDM), as downloaded from the GeoForschungsZentrum Postdam ftp server ftp://ftp.gfz-postdam.de/pub/home/ig/ops/.

Both pressure terms of the atmospheric EAMF correspond to the hydrostatic reaction of the ocean surface (Inverted Barometer oceans), which is known to be valid for time scales longer than 10 days.

Prior to the treatment, we apply a Vondrák (1977) smoothing to remove diurnal and sub-diurnal components of the atmospheric EAMF and oceanic EAMF of the OMCT model.

Geophysical AMF will be treated along with the geodetic excitation, derived from the daily C04 pole coordinate times series, produced by the International Earth Rotation and Reference Frame Service and downloaded from the server http://hpiers.obspm.fr/eop-pc/.

3 Prograde and retrograde terms and elliptical motion at a given frequency

Over a given time interval, complex coordinates (in the TRF) of the equatorial excitation can be decomposed into complex Fourier series reading

$$\chi(t) = \sum_{\sigma>0} a_\sigma^+ e^{i\sigma t} + a_\sigma^- e^{-i\sigma t} + \chi_0, \tag{5}$$

where a_σ^+ is the complex amplitude of the prograde (counterclockwise) term of angular frequency σ, a_σ^- is the analogue quantity specifying the retrograde term of same frequency; χ_0 is a constant term. In time domain, prograde and retrograde terms at a given frequency are determined by

$$\begin{aligned} \chi_\sigma^+(t) &= a_\sigma^+ e^{i\sigma t} = A_\sigma^+ e^{i\Phi_\sigma^+} e^{i\sigma t}; \\ \chi_\sigma^-(t) &= a_\sigma^- e^{-i\sigma t} = A_\sigma^- e^{i\Phi_\sigma^-} e^{-i\sigma t}, \end{aligned} \tag{6}$$

where A_σ^+, A_σ^- and Φ_σ^+, Φ_σ^- phrase the amplitude and phase, respectively. The total prograde and retrograde components in time domain are determined by adding the individual frequency terms of the Fourier decomposition:

$$\chi^+(t) = \sum_{\sigma>0} a_\sigma^+ e^{i\sigma t}; \quad \chi^-(t) = \sum_{\sigma>0} a_\sigma^- e^{-i\sigma t}. \tag{7}$$

Considering expressions (6), we see easily that prograde and retrograde terms at a given frequency are related by

$$\chi_\sigma^-(t) = \frac{a_\sigma^-}{(a_\sigma^+)^*} (\chi_\sigma^+(t))^* = \frac{A_\sigma^-}{A_\sigma^+} e^{i(\Phi_\sigma^+ + \Phi_\sigma^-)} (\chi_\sigma^+(t))^*. \tag{8}$$

On the other hand, the total contribution at frequency σ is $\chi_\sigma(t) = \chi_\sigma^+(t) + \chi_\sigma^-(t)$, that is

$$\begin{aligned} \chi_\sigma(t) = {} & e^{i(\Phi_\sigma^+ + \Phi_\sigma^-)/2} \\ & \times \left(A_\sigma^+ e^{i(\Phi_\sigma^+ - \Phi_\sigma^-)/2} e^{i\sigma t} + A_\sigma^- e^{i(-\Phi_\sigma^+ + \Phi_\sigma^-)/2} e^{-i\sigma t} \right). \end{aligned} \tag{9}$$

So, by doing the coordinate transformation $(x, y) \rightarrow (x', y')$ associated with the axial rotation of angle

$$\alpha_\sigma = \left(\Phi_\sigma^+ + \Phi_\sigma^-\right)/2, \tag{10}$$

the complex coordinate is multiplied by $e^{-i(\Phi_\sigma^+ + \Phi_\sigma^-)/2}$ and reads in the new system

$$\chi'_\sigma(t) = A_\sigma^+ e^{i(\Phi_\sigma^+ - \Phi_\sigma^-)/2} e^{i\sigma t} + A_\sigma^- e^{-i(\Phi_\sigma^+ - \Phi_\sigma^-)/2} e^{-i\sigma t}, \tag{11}$$

Consider $\theta_\sigma = (\Phi_\sigma^+ - \Phi_\sigma^-)/2$, then splitting real and imaginary parts of the former expression, we obtain

$$\chi'_\sigma(t) = (A_\sigma^+ + A_\sigma^-)\cos(\theta_\sigma + \sigma t) + i(A_\sigma^+ - A_\sigma^-)\sin(\theta_\sigma + \sigma t), \tag{12}$$

showing that equatorial component of frequency σ describes an elliptical path with the semi-major axis $A_\sigma^+ + A_\sigma^-$ directed along x' and the semi-minor axis $|A_\sigma^+ - A_\sigma^-|$ directed along y'. The orientation of the ellipse is determined with respect to the x-axis by the angle $\alpha_\sigma = (\Phi_\sigma^+ + \Phi_\sigma^-)/2$.

4 Example of the seasonal excitation

Practically the prograde and retrograde components at a given frequency are determined by fitting the model

$$\chi_\sigma(t) = (a_r^+ + i a_i^+) e^{i\sigma t} + (a_r^- + i a_i^-) e^{-i\sigma t} \tag{13}$$

to the observations, where a_r and a_i hold for real and imaginary parts, respectively, with the time origin taken as the epoch J2000. The estimated parameters a_r^+, a_i^+, a_r^-, a_i^- yield

$$\begin{aligned} A^+ &= \sqrt{(a_r^+)^2 + (a_i^+)^2} \quad \Phi^+ = \arctan \tfrac{a_i^+}{a_r^+} + \pi \left(1 - \mathrm{sign}(a_r^+)\right)/2 \\ A^- &= \sqrt{(a_r^-)^2 + (a_i^-)^2} \quad \Phi^- = \arctan \tfrac{a_i^-}{a_r^-} + \pi \left(1 - \mathrm{sign}(a_r^-)\right)/2 \end{aligned}. \tag{14}$$

Besides the diurnal and semi-diurnal oscillations out of the scope of this paper, the most prominent cycle of the excitation is seasonal. From year to year, its amplitude instability does not exceed 5 mas around a mean of 15 mas and its phase presents variation smaller than 30 degree. Therefore, the annual, semi-annual and terannual elliptical paths averaged over several years will be taken as a starting example.

The geodetic excitation is derived from the IERS C04 pole coordinate time series using the Wilson digital filter (Wilson 1985). The model (13) composed of the harmonics at 1, 1/2, 1/3 years and of linear trend is adjusted over the period 1997–2007. This seasonal-linear adjustment is redone for the corresponding angular momentum function (3) of the atmosphere (ECMWF) and the oceans (OMCT) and of the fresh water layer (LSDM). The seasonal components of $\chi(t)$ vectors in the equatorial plane are reconstituted in Fig. 1; in Table 1 we report the amplitude and phase of the annual prograde and retrograde terms. Apart the terannual term, the atmospheric contribution is strongly polarised towards ∼70°–90° in the x, y equatorial plane, as evidenced by studies of the 1970s and gathered in Sidorenkov (2009), Fig. 6.4; the hydrological AMF has almost a linear polarisation towards ∼90° East (annual term, other harmonics

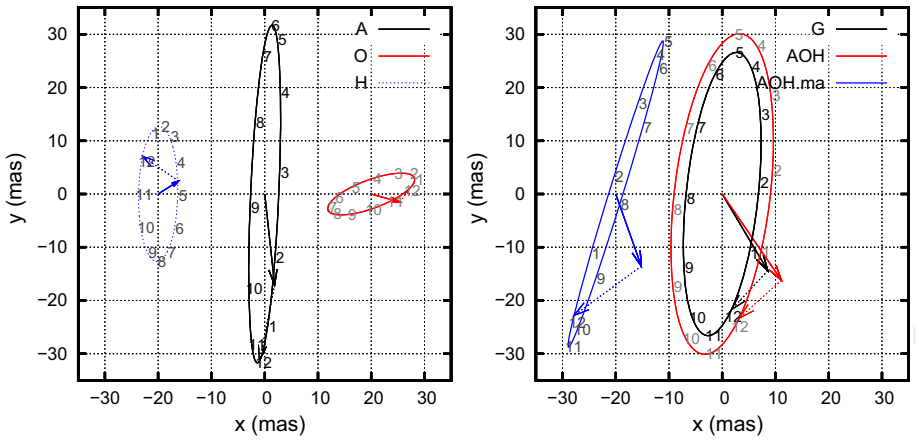

(a) Annual

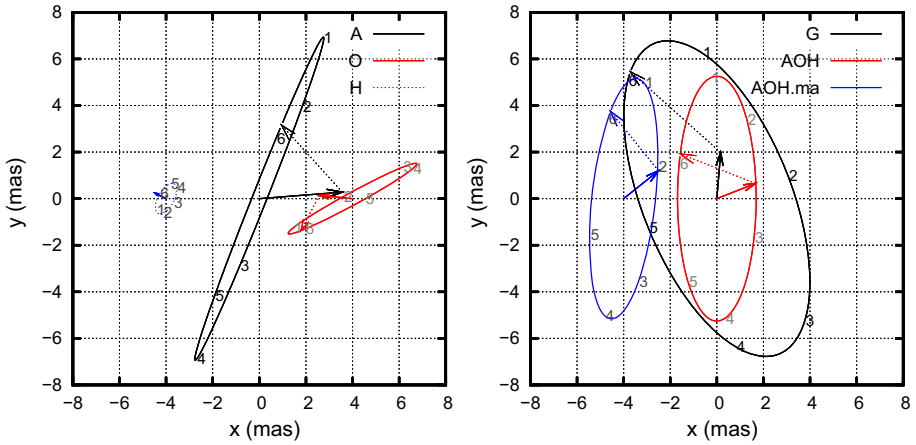

(b) Semiannual

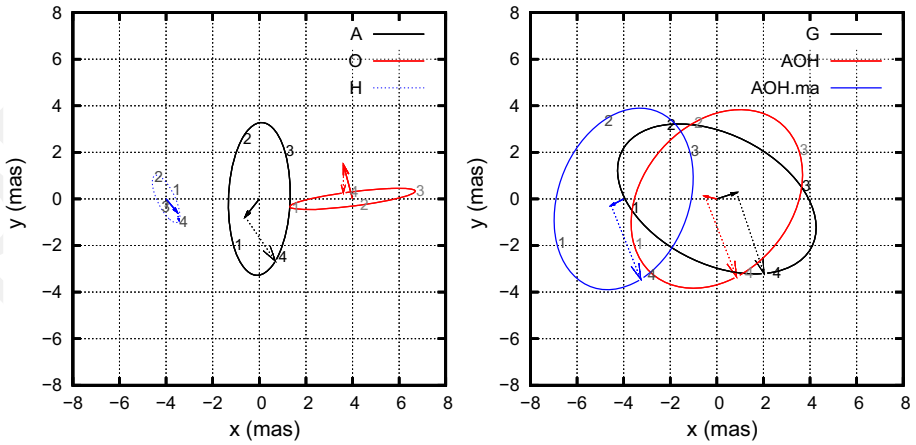

(c) Terannual

Fig. 1 Mean annual, semi-annual and terannual elliptical path of the polar motion excitation (period 1997–2007): deduced from pole coordinates (G) and associated with atmospheric A−ECMWF, oceanic O−OMCT, hydrological H−LSDM angular momentum series. We also displayed the total fluid layer contribution AOH and its matter term AOH.ma. *Plain arrow* amplitude and phase (at January 1) of the prograde terms, *dot arrows* those of the retrograde terms. *Numbers 1,2,3 . . .* along the annual ellipses correspond to the number of the elapsed month from the first of January

are below 1 mas). The ocean seasonal contribution is elliptically polarised towards 0°– 20°, but being three times smaller than the atmospheric effect, it is not surprising the geodetic excitation is also polarised like the atmospheric one. Notice also the good agreement between the total fluid layer contribution and geodetic elliptical path at the annual period, but disagreement at semi-annual and terannual periods.

Table 1 Annual components of the geodetic excitation and of the atmospheric, oceanic and hydrological AMF estimated over the period 1997–2007

	A^+ (mas)	Φ^+	A^- (mas)	Φ^-	$\alpha = (\Phi^+ + \Phi^-)/2$
χ_G	16.74 ± 0.72	$-59.3 \pm 2.5°$	9.98 ± 0.75	$227.0 \pm 4.3°$	84°
χ_O	5.65 ± 0.42	$-15.8 \pm 4.3°$	2.99 ± 0.47	$56.7 \pm 9.1°$	20°
χ_A	17.18 ± 0.40	$-83.8 \pm 1.3°$	14.54 ± 0.41	$258.8 \pm 1.7°$	87°
χ_{AO}	20.00 ± 0.64	$-68.6 \pm 1.8°$	11.82 ± 0.54	$264.2 \pm 2.6°$	100°
χ_{AOH}	19.64 ± 0.69	$-55.6 \pm 2.0°$	10.66 ± 0.70	$222.0 \pm 3.8°$	83°
χ_H	4.51 ± 0.10	$32.5 \pm 0.7°$	8.17 ± 0.10	$145.4 \pm 0.7°$	89°

Series A−ECMWF, O−OMCT and H−LSDM

5 Linear dependence of prograde and retrograde parts

According to (8) and (10), we have

$$\chi_\sigma^-(t) = \frac{A_\sigma^-}{A_\sigma^+}\, e^{i2\alpha_\sigma}\, \left(\chi_\sigma^+(t)\right)^* . \tag{15}$$

If the polarisation angle of the annual excitation, namely $\alpha \sim 80°$, tends to be the same for the other frequency components , then by adding all individual frequency components corresponding to the Eq. (15), we have

$$\chi^-(t) = e^{2i\alpha} \sum_\sigma \frac{A_\sigma^-}{A_\sigma^+}\, \left(\chi_\sigma^+(t)\right)^* , \tag{16}$$

where $\chi^-(t)$ is the total retrograde part of the excitation. Moreover, if the ratio $R_\sigma = A_\sigma^-/A_\sigma^+$ slightly depends on frequency, then we have the relation

$$\chi^-(t) \approx (\chi^+(t))^*\, R\, e^{2i\alpha}, \quad R > 0, \tag{17}$$

where $\chi^+(t)$ is the total prograde part of the excitation. The former relation means that prograde and retrograde parts are correlated in time domain. To determine this possible correlation, $\chi^-(t)$ and $\chi^+(t)$ are first reconstructed from the Complex direct Fourier transform of $\chi(t)$ over a given period: $\chi^-(t)$ is obtained by adding up the negative frequency terms and $\chi^+(t)$ by adding up the positive ones according to expressions (7). Then, considering $\alpha \sim 80°$, $\chi^-(t)$ is compared with $(\chi^+(t))^*\, R\, e^{i160°} \sim -R\,(\chi^+(t))^*$. So, as far as (17) is valid, we should have $\chi_x^-(t) \sim -R\chi_x^+(t)$ (equivalently the y components $\chi_y^-(t)$ and $\chi_y^+(t)$, which are nothing more than the x components out-of-phased by $\pi/2$ and $-\pi/2$, respectively, are related by $\chi_y^-(t) \sim R\chi_y^+(t)$).

The comparison of $\chi_x^-(t)$ and $-\chi_x^+(t)$ is shown in Fig. 2 for geodetic and the ECMWF-atmospheric excitations, split into two spectral bands by Vondrák (1977) low pass filter: seasonal and inter-annual band above 182 days (admittance $\geq$ 95 % for period larger than 182 days), and rapid band 2–182 days (admittance $\leq$5 % for periods larger than 182 days). The "rapid" band 2–182 days is shown on the whole year 2006, and the low frequency band from 1997 to 2007. Match between prograde and retrograde signals can

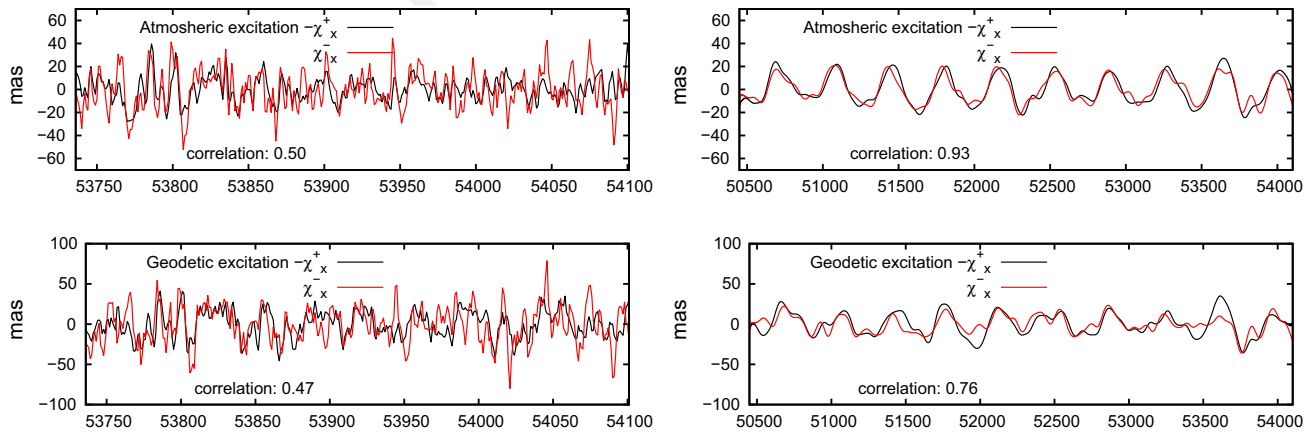

(a) 2-182 day band for the year 2006 **(b)** above 182 days, from 1997 to 2007

Fig. 2 Retrograde part $\chi_x^-(t)$ of the excitation against time compared with $-\chi_x^+(t)$. Geodetic (*bottom plot*) and atmospheric (*upper plot*) excitations split in two frequency bands: 2–182 days (**a**), and above 182 days (**b**). In both frequency bands, negative prograde variation along x axis reflects the retrograde ones. Time in Modified Julian Date

be noticed visually for each case, confirmed by correlation coefficients between $\chi_x^-(t)$ and $-\chi_x^+(t)$ of ~ 0.5 below 182 days and at least equal to 0.7 above 182 days.

The angle α giving the maximum correlation between $\chi^-(t)$ and $(\chi^+(t))^* e^{2i\alpha}$ can be derived by computing the complex correlation between $\chi^-(t)$ and $(\chi^+(t))^*$. Indeed, phase of the complex correlation is precisely 2α. The correlation amplitude CR and phase 2α are reported Table 2 for geodetic excitations for both triads of hydro-atmospheric series: A-ECMWF/O-OMCT/H-LSDM on one hand, and A-NCEP/O-ECCO/H-CPC on the other hand. Given the high sample size ($n \approx 3650$, corresponding to 10 years of data sampled at 1-day interval), a correlation coefficient above 0.3 has a p value lower than 0.01, meaning that such a correlation is significant at 99 % level and more. So, significant correlation pertains not only to geodetic ($\alpha = 75°$, CR = 0.50) and atmospheric excitations ($\alpha = 85°$, CR = 0.61 for ECMWF), but also to hydrological one ($\alpha = 90°$, CR = 0.81 for LSDM). The oceanic excitation is slightly less polarised ($\alpha = 50°$, CR = 0.33 for OMCT but $\alpha = 65°$, CR = 0.48 for ECCO).

Table 2 Complex correlation (amplitude CR and phase 2α) over the period 1997–2007 between conjugate prograde and retrograde excitations for geodetic excitation (G) and geophysical angular momentum functions: atmospheric (A), oceanic (O), hydrological (H), their sum (AO, AOH), corresponding matter (ma) and motion term (mo)

	Total excitation		Seasonal harmonics removed	
	CR	2α (°)	CR	2α (°)
G	0.50	2×75	0.46	2×75
A	0.61	2×85	0.42	2×80
	0.61	2×75	0.41	2×75
O	0.34	2×60	0.37	2×65
	0.48	2×70	0.48	2×75
H	0.80	2×90	0.63	2×95
	0.91	2×80	0.75	2×75
AO	0.42	2×85	0.34	2×75
	0.50	2×80	0.42	2×80
AOH	0.43	2×80	0.33	2×75
	0.54	2×80	0.44	2×80
A ma	0.77	2×75	0.48	2×75
	0.75	2×75	0.46	2×75
O ma	0.33	2×49	0.32	2×50
	0.48	2×70	0.48	2×70
AO ma	0.57	2×75	0.37	2×65
	0.64	2×75	0.48	2×75
AOH ma	0.55	2×70	0.34	2×65
A mo	0.09	2×40	0.11	2×65
	0.08	2×60	0.07	2×60
O mo	0.35	2×34	0.36	2×38
	0.27	2×34	0.21	2×38
AO mo	0.17	2×16	0.10	2×34
	0.04	2×55	0.03	2×80
AOH mo	0.17	2×16	0.10	2×34
	0.04	2×55	0.03	2×80

For fluid layer excitations, first line corresponds to the circulation models A-ECMWF/O-OMCT/H-LSDM, second line to the circulation models A-NCEP/O-ECCO/H-CPC. Phase of the complex correlation can be interpreted as the double of the elliptical polarisation angle α

The observed correlations partly result from the prominent annual oscillation, of which the elliptical motion presents the favoured orientation of $\sim 80°$ according to the former section. Yet, as the seasonal harmonic model of the former section is removed from the geodetic and fluid layer excitations, the correlations remain important (see Table 2). So, the polarisation is not only a feature of the regular seasonal part of signal, but also of its stochastic variations.

The separate analysis of matter and motion terms shows that the maximum correlation is obtained for the atmospheric (CR = 0.8) and hydrological (CR = 0.9) matter terms (hydrological excitation itself is a matter term), whereas prograde and retrograde parts of motion term are not significantly correlated (or slightly correlated for the ocean motion term). So, the elliptical polarisation towards $\sim 80°$ of the geodetic excitation can be attributed to the atmospheric and hydrological matter terms.

Geophysical trio A-ECMWF/O-OMCT/H-LSDM and A-NCEP/O-ECCO/H-CPC yield globally consistent results. Though, we notice significant differences pertaining oceanic and hydrological excitation (correlation amplitudes diverging by more than 0.1, and phases up to 40°).

6 Statistical distribution in spectral domain

As pointed out above, the elliptical polarisation of the excitation implies that prograde and retrograde circular oscillations at any frequency σ smaller than 0.5 cpd act to obey the condition

$$\chi_\sigma^-(t) \approx R_\sigma (\chi_\sigma^+(t))^* e^{2i\alpha_\sigma} \tag{18}$$

with privileged values of α_σ and R_σ. Considering spectral complex components $a_\sigma^+ = A_\sigma^+ e^{i\Phi_\sigma^+}$ and $a_\sigma^- = A_\sigma^- e^{i\Phi_\sigma^-}$ obtained by complex direct Fourier transform, the former relation reads also

$$r_\sigma = \frac{a_\sigma^-}{(a_\sigma^+)^*} \approx R_\sigma \, e^{2i\alpha_\sigma}. \tag{19}$$

Considering the geodetic excitation and the atmospheric ECMWF model, the R_σ and α_σ values were computed for the period 2000–2014, corresponding to more precise pole coordinates than prior to 2000 (Bizouard and Gambis 2008). The initial sample size of 2557 points sweeps the frequencies

from 2×10^{-4} to 0.5 cycle/day. But some of these ratio are not significant in light of the uncertainty which affects spectral coefficients. They are eliminated according to the uncertainty level of the geodetic excitation. This one is estimated by multiplying the spectral uncertainty of the pole coordinates by the inverse transfer function amplitude $|T(\sigma)^{-1}|$ (see Eq. 4). According to Zotov and Bizouard (2012) (see Bizouard 2014 for more details), the pole coordinates derived with GNSS techniques have a spectral uncertainty obeying a Flicker noise law

$$\varepsilon(f) \approx \frac{0.04\,\mathrm{mas}}{\sqrt{Pf}}, \tag{20}$$

where f means the frequency and P the period of study. Thus, the geodetic excitation has the spectral error

$$\varepsilon_\chi(f) = \frac{0.04\,\mathrm{mas}}{\sqrt{Pf}} \left| \frac{\tilde{f}_c}{f - \tilde{f}_c} \right|, \tag{21}$$

where $\tilde{f}_c = \tilde{\sigma}_c / 2\pi$ is the complex Chandler frequency. The ratio $r_\sigma = a_\sigma^- / (a_\sigma^+)^*$ is considered as far as the amplitude A_σ^+ is larger than $\varepsilon_\chi(f)$, and frequencies do not satisfying this criteria are rejected. The same criteria is applied to fluid layer excitations, for which we do not have sound assessment of the errors.

For the selected frequencies, the complex ratio $r_\sigma = R_\sigma\, e^{2i\alpha_\sigma}$ is estimated. In Fig. 3, we plot R_σ and α_σ along frequency σ for geodetic (G), ECMWF-atmospheric (A) and combined ECMWF-atmospheric/OMCT-oceanic (AO) excitations. This manifests privileged distributions $1 \lesssim R_\sigma \lesssim 2$ and $50° \lesssim \alpha_\sigma \lesssim 150°$ whatsoever the frequency band, except for frequencies approaching the Nyquist frequency of 0.5 cpd of the polar motion series. In reason of this proximity, the shift of α_σ towards 180° noticed in geodetic excitation could be considered as doubtful, but it is accounted for the combined AO excitation, of which the initial sampling is 4-daily (before low pass filtering and interpolation at the daily time step).

A complementary insight is brought by the histograms of R_σ and α_σ distributions, displayed in Fig. 4 for the geodetic and atmospheric excitations. The histograms corresponding to the combined fluid layer excitations (AO or AOH) are very similar to the one of χ_G, therefore are not displayed. The statistic distribution is envisaged in two cases: (i) for the whole spectrum encompassing periods from 2 days to 14 years; (ii) for periods beyond 10 days (frequency smaller than 0.1 cpd).

With the mean value $\mu \sim 80°$ and standard deviation $\sigma \sim 40°$, the histogram of α_σ has a bell form, which looks like the corresponding normal distribution $\mathcal{N}(\mu; \sigma)$. The agreement with normal law seems to be reinforced by selecting frequencies below 0.1 cpd.

We found empirically that the amplitude ratio R_σ can be approached by the gamma probability law

$$f_\Gamma(x, k, \theta) = e^{-x/\theta} \frac{x^{k-1}}{\theta^k \Gamma(k)}, \tag{22}$$

where $\Gamma(k) = \int_0^\infty t^{k-1} e^{-t} \mathrm{d}t$ is the Euler Gamma function, θ is the scale parameter and k the shape parameters, which are related to the mean value μ and the standard deviation σ of the distribution by $\mu = k\theta$, $\sigma^2 = k\theta^2$ ($\theta = \sigma^2/\mu$). In the studied case, the parameters k and θ are determined

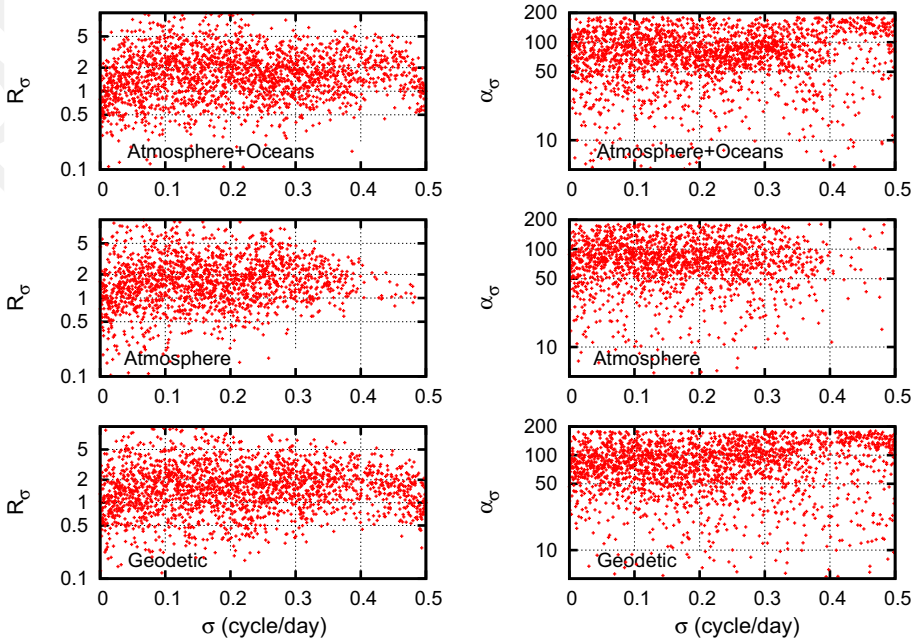

Fig. 3 Plots of R_σ (retrograde to prograde amplitude ratio) and α_σ in degree (elliptical orientation with respect to x-axis) as a function of the frequency σ for the geodetic, ECMWF-atmospheric, and ECMWF-atmospheric/OMCT-oceanic excitations

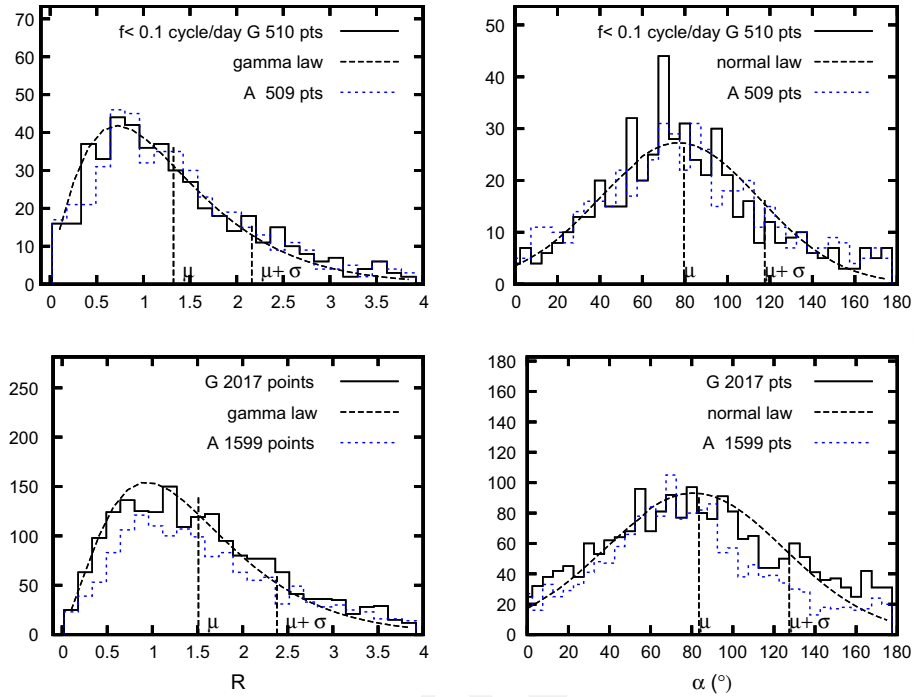

Fig. 4 Histograms of the ratio $R_\sigma = |a_\sigma^- / (a_\sigma^+)^*|$ and of α_σ for the geodetic and atmospheric excitation. *Left panels* R_σ between 0 and 4 with 0.04 bin-width and gamma distribution law corresponding to the mean $\mu \sim 1.5$ and standard deviation $\sigma \sim 1$ of the geodetic excitation (maximum for 1). *Right panel* α_σ between 0 and 180° with 5° bin-width, and normal law corresponding to the mean $\mu \sim 80°$ and standard deviation $\sigma \sim 40°$ of the geodetic excitation. *Upper plots* correspond to the frequencies lower than 0.1 cpd. Initial sample size of 2557 points (before elimination of not significant terms)

Table 3 Goodness of fit of R_σ and α_σ histograms by gamma and normal law, respectively (having the mean and standard deviation of the corresponding samples)

	R_σ (against gamma law)		α_σ (against normal law)	
	χ_2^e	$P(\chi_2 \geq \chi_2^e)\%$	χ_2^e	$P(\chi_2 \geq \chi_2^e)\ \%$
G	4.23	0.00	6.12	0.00
A	3.60	0.00	6.49	0.00
G $f < 0.1$ cpd	1.26	18.25	2.93	0.00
A $f < 0.1$ cpd	1.44	8.29	1.58	1.80

The lower is the probability $P(\chi_2 \geq \chi_2^e)$, the poorer is the fit. Below 0.1 %, it can be rejected

by $\mu \sim 1.5$ and $\sigma^2 \sim 1^2$. Maximum is reached for equal amplitude ratio.

The Pearson's Chi-squared test allows us to test the proposed probability laws. For both α_σ and R_σ distributions, we estimated reduced Chi-squared, that is

$$\chi_2^e = \frac{1}{N-3} \sum_i \frac{(O_i - E_i)^2}{E_i},$$

where N is the number of bins ($N = 36$ for α_σ, $N = 25$ for R_σ), O_i is the observed distribution (expected outcome frequencies), E_i is the expected theoretical frequency for bin i, asserted by the null hypothesis (the degree of freedom is the number of bins N minus 3 constraints: same mean, standard deviation and number of bins for sample and tested distributions). Both χ_2^e and probability that χ_2 is larger than the estimated value are reported in Table 3. The null hypothesis is accepted if $\chi_2^e \sim 1$, cases with $2 \leq \chi_2^e \leq 3$ are questioned, and those with $\chi_2^e \geq 3$ are rejected. So the ratio R_σ for $f < 0.1$ cpd clearly obeys the gamma law, but the slight skewness and sharpness of the α_σ distributions, except in the case A, $f \leq 0.1$ cpd, make them diverge from the normal law.

Considering the geodetic excitation for $f \leq 0.1$ cpd, the mean of α_σ becomes 75° with a number of occurrences (∼44) significantly higher than the value expected from the normal distribution (∼28), given that the expected value obeys a Poisson probability law with a standard deviation of $\sim\sqrt{28} \approx 5$. This makes the elliptical orientation of 75° even more probable than in the case of a normal distribution.

The corresponding statistic distributions for the hydrological AMF, not represented here, are at odds with the atmospheric and geodetic ones: to R_σ corresponds a gamma probabilistic distribution centred on 1; the angular distribution α_σ, centred on ∼95° follows a much sharper and asymmetric bell. This sharpness results from the fact that the hydrological excitation results from seasonal and inter-annual processes located on continental regions, making it much more polarised than the rapid components observed in geodetic and atmospheric/oceanic excitations (see Fig. 2).

The gamma distribution R_σ centred on 1.5 and the bell form centred on ∼75° were also tracked down for the oceanic excitation. By selecting frequency $f < 0.1$ cpd, the influence of the matter term (resulting from bottom oceanic pressure variations) is highlighted; this shifts the maximum of oceanic α_σ towards ∼50°, as expected from Table 2, and causes a strong skewness.

Though, as the fluid layer excitation is dominated by the atmospheric contribution, geodetic statistical distributions mostly reflect the atmospheric ones.

7 Discussion

Complementary methods (correlation in time domain, statistical distribution in spectral domain) show that the retrograde and prograde parts of the polar motion excitation are related. This reflects not only an elliptical polarisation towards 80° East (India, Tibet, Central Siberia), equivalently 180° + 80° = 260° East or 100° West (Central Northern America), but also a privileged amplitude ratio of about 1.5 between retrograde and prograde terms (not the case of the annual terms) with predominance of the retrograde terms. These characteristics clearly result from the air and continental water mass redistributions, and are explained by the matter term of their associated angular momentum.

Atmospheric angular momentum function (AMF) polarisation towards 80° East can be explained as far as continental zones of maximal hydro-atmospheric mass redistribution, whatsoever the frequency band, are close to a great meridian circle, namely the one of longitude ∼80 ± 10° East. Actually, the largest continental contribution to the pressure term is located over Eurasia and North America, as it has been documented in Nastula et al. (2009) for several spectral bands namely, interannual (730–1825 days), annual (230–450 days), semiannual (150–230 days), terannual (90–150 days), and subseasonal (30–90 days). In the Chandler band, the pressure term mostly results from longitudinal band 0°–145° (Eurasia) (Zotov and Bizouard 2014).

Moreover, major contribution to the hydrological AMF in the seasonal band comes form basins located in South-Eastern Asia, South America and Northern Australia, and southern Africa (Nastula et al. 2014); apart from the latest, these regions are near the great circle of longitude ∼80 ± 10°, so that the hydrological AMF tends to be maximum by crossing the great circle of longitude ∼80 ± 10°.

Though the result is less significant, the oceanic excitation also presents an overall elliptical polarisation towards a more western longitude, namely ∼65–75 ± 10°-East for a reason which is not elucidated, but this does not influence much the polarisation of the geodetic excitation.

The gamma law of the A^-/A^+ distribution is more difficult to be accounted for. The predominance of the retrograde terms could partly result from the atmospheric normal mode Ψ_3^1, propagating towards the west (thus retrograde) with a period of about 10 days (see e.g. Brzeziński et al. 2002), thus enhancing retrograde components of pressure term around 0.1 cycle/day. As elliptical fixed-frequency components tend to adopt the ratio $A^-/A^+ \sim 1.5$, their ellipticity, defined as the relative difference between semi-major and semi-minor axis, that is

$$\frac{A^+ + A^- - |A^+ - A^-|}{A^+ + A^-} = 1 - \frac{|1 - A^-/A^+|}{1 + A^-/A^+}$$

tends to take the value 0.8.

The substantial conclusion of this study is the following: we detected a linear statistical dependence between retrograde and prograde parts of the polar motion excitation in time domain; equivalently elliptical fixed-frequency components act to take a favoured orientation (80° East) and ellipticity (0.8), and thus conspire towards an overall elliptical polarisation. This results from the air and continental water mass redistributions according to a process which is not fully elucidated. Future study has also to investigate how this polarisation is reflected by polar motion.

Acknowledgments We are grateful to our three reviewers for their careful analysis, which permitted to improve the quality of this study. We are especially indebted to Leonid Zotov for having carried out some computational check.

References

Barnes RTH, Hide R, White AA, Wilson CA (1983) Atmospheric angular momentum fluctuations, length-of-day changes and polar motion. Proc R Soc Lond A 387:31–73

Bizouard C (2014) Le mouvement du pôle de l'heure au siècle. Presses Académiques Francophones, p 284

Bizouard C, Gambis D (2008) The combined solution C04 for Earth Orientation Parameters, recent improvements. In: Drewes H (ed) Series International Association of Geodesy Symposia 134. Springer Verlag series, p 330. ISBN: 978-3-642-00859-7

Brzeziński A (1994) Polar motion excitation by variations of the effective angular momentum function, II: extended model. Manuscr Geod 19:157–171

Brzeziński A, Bizouard C, Petrov S (2002) Influence of the atmosphere on Earth rotation: what new can be learnt from the recent atmospheric angular momentum estimates? Surv Geophys 23:33–69

Lambeck K (1980) The Earth's variable rotation : geophysical causes and consequences. Cambridge University Press

Munk WH, Mac Donald G (1960) The rotation of the Earth. Cambridge University Press, Cambridge

Nastula J, Salstein D, Kolaczek B (2009) Patterns of atmospheric excitation functions of polar motion from high resolution regional sectors. J Geophys Res 114:B04407. doi:10.1029/2008JB005605

Nastula J, Salstein D, Gross R (2014) Regional Multi-fluid-based geophysical. excitation of polar motion. In: Rizos C, Willis P (eds) Earth on the edge: science for a sustainable planet. International

Association of Geodesy Symposia 139. Springer-Verlag, Berlin, Heidelberg (2014). doi:10.1007/978-3-642-37222-3-62

SBA (2015) Website of the IERS Special bureau for the atmosphere. http://ftp.aer.com/pub/anon_collaborations/sba/

SBH (2015) WEB site of the IERS special bureau for hydrology. http://geophy.uni.lu/ggfc-hydrology.html

SBO (2015) WEB site of the IERS special bureau for the oceans. http://geophy.uni.lu/ggfc-oceans.html

Sidorenkov N (2009) The interaction between Earth's rotation and geophysical processes, Wiley-VCH Verlag GmbH &Co., Chapter 6, p 113–118. ISBN 978-3-527-40875-7

Vondrák J (1977) Problem of smoothing observational data II. Bull Astron Inst Czech 28:84–89

Wilson C (1985) Discrete polar motion equation. Geophys J R Astron Soc 80(2):551–554

Zotov L, Bizouard C (2012) On modulations of the Chandler wobble excitation. J Geodyn. doi:10.1016/j.jog.2012.03.010

Zotov L, Bizouard C (2014) Regional atmospheric influence on the Chandler wobble. Adv Space Res. Elsevier. doi:10.1016/j.asr.2014.12.013